

Functional MRI Using Regularized Parallel Imaging Acquisition

Fa-Hsuan Lin,^{1*} Teng-Yi Huang,^{1,2} Nan-Kuei Chen,³ Fu-Nien Wang,^{1,4} Steven M. Stufflebeam,¹ John W. Belliveau,¹ Lawrence L. Wald,¹ and Kenneth K. Kwong¹

Parallel MRI techniques reconstruct full-FOV images from undersampled k -space data by using the uncorrelated information from RF array coil elements. One disadvantage of parallel MRI is that the image signal-to-noise ratio (SNR) is degraded because of the reduced data samples and the spatially correlated nature of multiple RF receivers. Regularization has been proposed to mitigate the SNR loss originating due to the latter reason. Since it is necessary to utilize static prior to regularization, the dynamic contrast-to-noise ratio (CNR) in parallel MRI will be affected. In this paper we investigate the CNR of regularized sensitivity encoding (SENSE) acquisitions. We propose to implement regularized parallel MRI acquisitions in functional MRI (fMRI) experiments by incorporating the prior from combined segmented echo-planar imaging (EPI) acquisition into SENSE reconstructions. We investigated the impact of regularization on the CNR by performing parametric simulations at various BOLD contrasts, acceleration rates, and sizes of the active brain areas. As quantified by receiver operating characteristic (ROC) analysis, the simulations suggest that the detection power of SENSE fMRI can be improved by regularized reconstructions, compared to unregularized reconstructions. Human motor and visual fMRI data acquired at different field strengths and array coils also demonstrate that regularized SENSE improves the detection of functionally active brain regions. Magn Reson Med 54: 343–353, 2005. © 2005 Wiley-Liss, Inc.

Key words: fMRI; SENSE; EPI; parallel MRI; brain

To study the human functional brain, functional MRI (fMRI) was introduced to map brain activity (1–3). The combination of high spatial resolution (millimeters), the use of cerebral blood as an endogenous contrast agent (4,5), and the ease of imaging underlying anatomy has made fMRI a widely used tool for mapping brain function. Typically, echo-planar imaging (EPI) (6) is used in fMRI to achieve sufficient spatiotemporal resolution. Owing to ad-

vances in MRI facilities, including high slew-rate gradients, high-quality radiofrequency (RF) coils, dedicated pulse sequence design, and image reconstruction algorithms, a temporal resolution of 1–2 s and a spatial resolution of 3–5 mm can be achieved simultaneously for whole-brain fMRI. However, the spatiotemporal resolution of fMRI is limited by technological challenges, safety concerns regarding acoustic noise, peripheral nerve stimulation, and the specific absorption rate (SAR) of tissue (7).

In 1990 the RF coil array was introduced to improve the signal-to-noise ratio (SNR) of an image (8). In practice, multiple sets of data are obtained from an RF coil array that consist of spatially distinct observations of MRI signals, modulated by individual coil sensitivity profiles. Therefore, instead of combining individual coil images for higher SNR or larger field of view (FOV) in MRI, it is possible to use multiple receivers in the array to reconstruct full-FOV images from the incomplete k -space acquisition. To restore full-FOV images from undersampled k -space data or aliased images, approaches involving both the k -space domain (simultaneous acquisition of spatial harmonics (SMASH)) (9) and the image domain (sensitivity encoding (SENSE)) (10) have been proposed. Such parallel MRI techniques can reduce the imaging scan time and thus improve the temporal resolution. Alternatively, parallel MRI can be used to increase the image spatial resolution within the same amount of acquisition time. Additional benefits of the parallel MRI technique include reduced susceptibility artifact due to reduced readout duration, decreased geometrical distortion due to increased phase-encoding bandwidth (11,12), and lower EPI acoustic noise due to reduced gradient switching (13). Several groups have applied SENSE using EPI (14–16) or principles of echo-shifting with a train of observation (PRESTO) (17) pulse sequences to fMRI experiments to gain the advantages of parallel MRI.

However, parallel MRI also has some disadvantages. For example, the SNR of an image is usually lower due to 1) the reduced data sample and 2) the instability involved in the unfolding operation. The loss of SNR in parallel imaging due to the first reason is inevitable because of the reduced data samples compared to the traditional k -space acquisitions. Reason 2 is closely related to the geometric layout of the elements of an RF array, which may not be optimal to provide sufficient independent information from all elements in the array to unfold the aliased image. Since the formation and reconstruction of parallel MRI were formulated as a linear equation (18), we could employ the Tikhonov regularization technique (19) to minimize the noise amplification in the reconstruction of a full-FOV image with an L-curve based regularization

¹Massachusetts General Hospital, Department of Radiology, MGH-HMS-MIT, Athinoula A. Martinos Center for Biomedical Imaging, Charlestown, Massachusetts, USA.

²Department of Electrical Engineering, National Taiwan University of Science and Technology, Taipei, Taiwan.

³Department of Radiology, Brigham and Women's Hospital, Boston, Massachusetts, USA.

⁴Department of Electrical Engineering, National Taiwan University, Taipei, Taiwan.

Grant sponsor: National Institutes of Health; Grant numbers: R01 HD040712; R01 NS037462; P41 RR14075; Grant sponsor: Mental Illness and Neuroscience Discovery Institute (MIND).

*Correspondence to: Fa-Hsuan Lin, Athinoula A. Martinos Center for Biomedical Imaging, Bldg. 149, 13th Street, Mailcode 149-2301, Charlestown, MA 02129. E-mail: fhlin@nmr.mgh.harvard.edu

Received 12 October 2004; revised 25 February 2005; accepted 26 February 2005.

DOI 10.1002/mrm.20555

Published online in Wiley InterScience (www.interscience.wiley.com).

© 2005 Wiley-Liss, Inc.

(20,21). Our previous study of regularized SENSE imaging focused on mitigating the SNR loss in anatomical/structural images, especially at high acceleration rate cases, but not in dynamic studies. In this paper we focus on the effect of the regularization process on dynamic imaging and an fMRI time series. In our previous paper (20), we noted that replicates of prior image features were present in the SENSE reconstructed images when the regularization was high. Replication of prior images may hinder our ability to distinguish brain activation from baseline brain activity, because fMRI relies on the dynamic information obtained from different imaging time points to differentiate brain activity. Since the blood oxygen level-dependent (BOLD) contrast in fMRI is usually low (e.g., only 10% on a 7T high-field scanner) (22), a reduction of the functional contrast-to-noise ratio (CNR) by regularization is undesirable. On the other hand, the noise associated with the SENSE unfolding is also reduced in the regularized SENSE reconstruction (20). A direct comparison of the CNR performance of SENSE functional MRI with and without regularization has not been systematically investigated. In this work we performed parametric simulations to study the effect of regularization on parallel MRI acquisitions in the context of fMRI. We also used visual and motor fMRI data acquired at 1.5T and 3T scanners to quantitatively study the impact of regularized SENSE reconstruction on the fMRI detection power. A regularized SENSE fMRI strategy is proposed to obtain high detection power in fMRI studies.

MATERIALS AND METHODS

Regularized and Unregularized SENSE Image Reconstruction Using In Vivo Sensitivity

Mathematically, the formation of aliased images from multiple receivers can be formulated as a linear operation to “fold” the full-FOV spin density images (18):

$$\tilde{\mathbf{y}} = \mathbf{S}\tilde{\rho}_{full} \quad [1]$$

where $\tilde{\mathbf{y}}$ is the vector formed from vertical concatenation of the pixel intensities recorded by each receiver (folded image), and $\tilde{\rho}_{full}$ is the vector formed from the full-FOV image. The encoding matrix \mathbf{S} consists of the vertical stacks of the product of the aliasing operation due to subsampling of the k -space data and the coil-specific sensitivity modulation over the image. The goal of the parallel MRI reconstruction is to solve for $\tilde{\rho}_{full}$ given our knowledge of \mathbf{S} . While Eq. [1] is expressed in the image domain SENSE approach (10), similar linear relationships are formed in the k -space-based SMASH (9,23) method.

Instead of using the traditional SENSE formulation shown in Eq. [1], we adopted an in vivo sensitivity reconstruction (23) to avoid potential errors due to misestimation of the coil sensitivity. Using in vivo sensitivity reconstruction, we estimated the “spin density ratio” in the full-FOV reference scan and SENSE accelerated scan:

$$\tilde{\mathbf{y}} = \mathbf{A}\tilde{\mathbf{x}} \quad \tilde{\mathbf{x}} = \frac{\tilde{\rho}_{acc}}{\tilde{\rho}_{full}} \quad [2]$$

where the encoding matrix \mathbf{A} is the vertical stacks of the product of the aliasing operation and full-FOV coil element images, and $\tilde{\rho}_{acc}$ and $\tilde{\rho}_{full}$ indicate the full-FOV spin density in the SENSE accelerated scan and full-FOV reference scan, respectively. Practically, in vivo sensitivity formulation only estimates the ratio of spin density between accelerated and full-FOV reference scans. Thus, it avoids the estimation of the coil sensitivity profile, as required in conventional SENSE reconstruction. Since fMRI experiments mostly focus on the within-voxel dynamic BOLD contrast, which is a balance between T_2^* changes between oxy-/deoxyhemoglobin and oxyhemoglobin inflow effects, an in vivo sensitivity formulation serves to differentiate the active from the baseline brain states. Note that no additional body coil scanning is used to acquire the coil sensitivity profiles when the in vivo sensitivity method is employed. The full-FOV reference images are used as the coil sensitivity. The experimental procedure used to acquire such reference images is presented in the following section.

To solve for the full-FOV image, the encoding matrix is inverted by means of a least-squares estimation (10). To quantify the noise sensitivity of the parallel imaging reconstruction, the amplification of the noise power (g -factor) is derived (10). In a recent study (20) we proposed the use of full-FOV prior information to stabilize the reconstruction of a SENSE image. In the following section we present a segmented EPI acquisition scheme to acquire the composition of all EPI segments as the prior information. Given the prior information $\tilde{\mathbf{x}}^0$ for the solution $\tilde{\mathbf{x}}$, we can use Tikhonov regularization to minimize the following cost function to solve for the full-FOV regularized reconstructed image:

$$\tilde{\mathbf{x}}^\lambda = \arg \min_{\tilde{\mathbf{x}}} \{ \|\tilde{\mathbf{A}}\tilde{\mathbf{x}} - \tilde{\mathbf{y}}\|_2 + \lambda^2 \|\mathbf{L}(\tilde{\mathbf{x}} - \tilde{\mathbf{x}}^0)\|_2 \} \quad [3]$$

where λ^2 is the regularization parameter, \mathbf{L} is a positive semidefinite linear transformation, λ^2 denotes the prior information about the solution $\tilde{\mathbf{x}}^0$, and $\|\bullet\|_2$ represents the L-2 norm. The regularization parameter can be estimated by the L-curve technique (21). The solution of Eq. [3] and the associated g -factor were derived previously.

Reference and Accelerated Image Acquisition Using Segmented EPI

We used a segmented gradient-echo EPI sequence (24,25) to acquire dynamic data. Figure 1 shows a schematic k -space trajectory with an EPI factor of 4. In segmented EPI, each EPI segment is acquired individually and sequentially with a distinct prephase shift. For each EPI segment, due to insufficient sampling along the phase-encoding direction to satisfy the Nyquist sampling criterion, the Fourier reconstruction of an individual EPI segment yields an aliased image. To avoid aliasing, multiple EPI segments can be combined by appropriate prephasing in each EPI segment in the phase-encoding direction, such that the k -space gap between the nearest two EPI phase-encoding lines is equal to the inverse of the FOV. This image reconstruction approach is termed “composition reconstruction”.

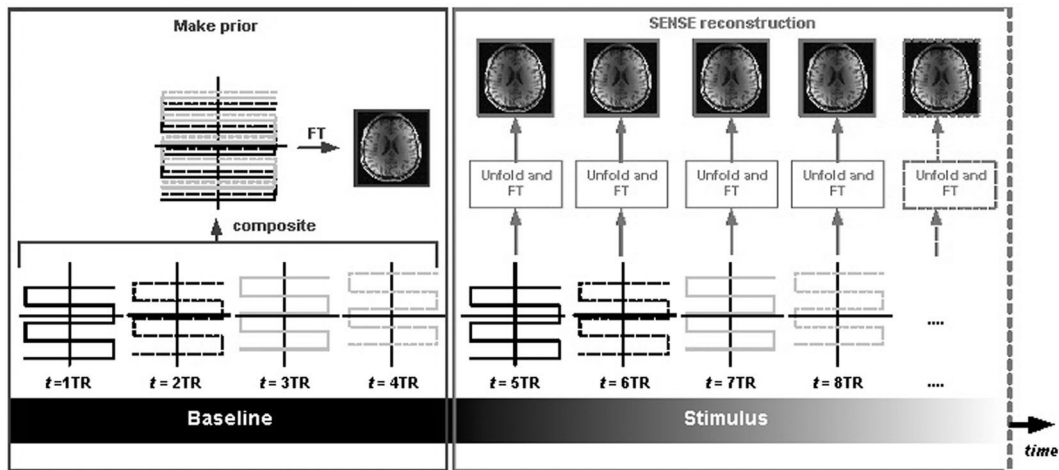


FIG. 1. **a**: Schematic diagram of a four-segment EPI acquisition. In the baseline acquisition, the combination of all four EPI segments makes the prior for the subsequent SENSE reconstructions with identical bandwidth and read-out time and associated geometrical distortion and susceptibility artifact. In the actual fMRI experiment, each EPI segment generates a full-FOV image using SENSE reconstruction.

tion” in this paper, in order to differentiate it from the SENSE reconstructions described in the following text.

In SENSE MRI, instead of composition reconstruction, each EPI segment yields an aliased image from the individual element of the RF array. Subsequent SENSE unfolding can restore a full-FOV image from single EPI segment in multiple RF array coils using the TSENSE or UNFOLD technique to achieve temporal resolution enhancement (25,26). In regularized SENSE imaging reconstruction, the prior full-FOV reference image is crucial, since it biases the reconstruction of the SENSE acquisitions. Here we propose to use the composition reconstruction at the first n TR of the n -segment segmented EPI sequence to acquire the reference image. The n -segment segmented EPI is suitable for achieving n -fold acceleration, as shown in Fig. 1. The full-FOV reference image should be acquired during the baseline period of the fMRI experiment without presenting any stimulus in order to avoid a reduction of contrast between active and baseline brain states in the reconstructed image. Such a full-FOV reference image will have image distortion and susceptibility artifacts identical to those of the SENSE reconstructed image, since both have identical bandwidths and readout times.

Simulations

We tested the performance of SENSE reconstructions with and without regularization by parametric simulations. To simulate the fMRI time series with SENSE acquisitions, we acquired baseline EPI images on a 3T scanner (Siemens Medical Solution, Inseln, NJ, USA) with an eight-channel linear phased-array coil wrapped around the whole brain circumferentially. Imaging acquisition used a 2D gradient-echo EPI sequence with the following parameters: TR = 2000 ms, TE = 50 ms, flip angle = 90°, slice thickness = 5 mm with 0.5-mm gap, 14 slices, FOV = 192 mm × 192 mm, and image matrix = 64 × 64. The array coil geometry and a typical EPI image, along with the spatial distribution of the SNR, are shown in Fig. 2. The SNR of the EPI image was calculated from the combined EPI im-

ages from all channels of the RF array by determining the ratio between the image intensity and the background standard deviation (SD).

In the first simulation, a time series of 100 images was created artificially with maximal SNR = 150 at the periphery of the cortex, which matched our experimental result shown in Fig. 2. On 50 images, we artificially implanted a BOLD contrast of 2% at 4 pixels (2 × 2) around the occipital lobe to simulate the functional activation. Time stamps with implanted BOLD contrast were used as the paradigm file in calculating functional activation using a t -test (27) after SENSE unfolding. The k -space data of the images were decimated to simulate 2.67-fold SENSE acceleration (keeping three k -space lines in eight contiguous k -space lines), and 4.00-fold SENSE acceleration (keeping every fourth line in four contiguous k -space lines).

In the second simulation, a time series of 100 images was created synthetically with maximal SNR = 150. Using zero-mean Gaussian noise, we adjusted the variance for all voxels such that the spatial distribution of SNR of all voxels matched the SNR illustrated in Fig. 2. Different realizations of the noise (as described above) were generated in each simulation. In a manner identical to the first simulation, 50 baseline images and 50 active images were simulated in each time series. Here we varied three parameters in each simulated data set: 1) BOLD contrasts were changed parametrically from 1%, 2%, 5%, to 10%; 2) the size of the active areas was change from 4 pixels (36 mm²), to 16 pixels (144 mm²), and to 64 pixels (576 mm²); and 3) the SENSE acceleration rates were changed from 2.00-fold, to 2.67-fold, and to 4.00-fold. In each combination of the simulation parameters, 50 realizations of the time series were generated. Both regularized and unregularized SENSE reconstructions were calculated to restore the full-FOV unaliased fMRI time series. To quantify the detection power, we performed receiver-operating characteristic (ROC) analysis (see section below). The ROC analysis results were averaged over 50 realizations of the simulated data for each combination of simulation parameters.

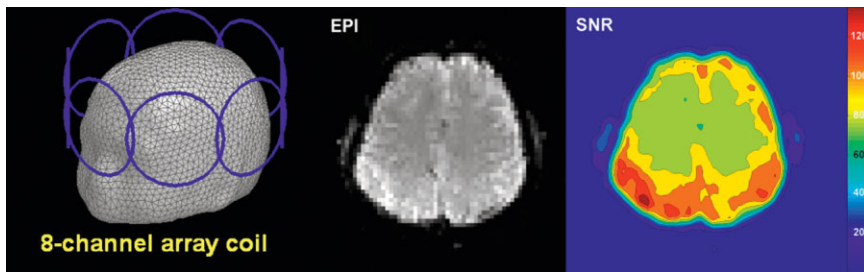


FIG. 2. Left: The layout of the eight-channel array coil. Middle: A typical EPI image using a sum-of-squares combination from the eight-channel array. Right: The spatial distribution of the SNR of the EPI image.

3T Visual fMRI Experiment

One set of blocked-design visual fMRI data was acquired from a 3T scanner with an eight-channel phased-array coil as described above. A healthy subject was recruited for the study after approval was obtained from the institutional review board, and the subject gave informed consent. A visual stimulus (4-Hz checkerboard) was presented using E-PRIME software (Psychology Software Tools, Inc., Pittsburgh, PA, USA). The visual stimulus was designed to display either continuous checkerboards at 4 Hz flashing for 30 s (“on” condition), or 30 s fixation (“off” condition). Three “off” conditions and two “on” conditions were alternatively presented to the subject, starting with the “off” condition. The imaging acquisition used a 2D gradient-echo EPI sequence with the following parameters: TR = 2000 ms, TE = 50 ms, flip angle = 90°, slice thickness = 5 mm with 0.5-mm gap, 14 slices, FOV = 200 mm × 200 mm, and image matrix = 128 × 128. In addition to single-shot full phase-encoding data (60 volumes with 24 “on” and 36 “off” conditions; 10 dummy scans), we collected three-segment EPI data (20 volumes in composition reconstruction with 8 “on” and 12 “off” conditions; 10 dummy scans) and four-segment EPI data (15 volumes in composition reconstruction with six “on” and nine “off” conditions; 10 dummy scans). The phase encoding was along the anterior–posterior direction.

1.5T Motor fMRI Experiment

Blocked-design motor fMRI data were acquired from a 1.5T (GE Medical, Milwaukee, WI, USA) scanner using a four-channel head array (Nova Medical, Wakefield, MA, USA). The array was wrapped around the periphery of the whole head with four equally curved rectangular surface coils. One subject participated in the study after giving signed informed consent, and the experiment was approved by the institutional review board. The subject was asked to perform the finger flexion task using his thumb and other fingers of his right hand alternatively during the “on” block for 30 s continuously. The finger flexion was self-paced, and the subject randomly chose the fingers for the flexion task. Following the “on” block, the subject was asked to remain still without making any hand movement during the “off” block for 30 s. Two “on” and two “off” blocks were recorded. We used a 2D gradient-echo EPI sequence with the following parameters: TR = 2500 ms, TE = 50 ms, flip angle = 90°, slice thickness = 6 mm without gap, eight slices, FOV = 240 mm × 240 mm, and image matrix = 128 × 128. Two sets of phase-encoding data were collected: full phase-encoding data (60 volumes

with 24 “on” and 36 “off” conditions; 10 dummy scans), and two-segment EPI data (30 volumes with 12 “on” and 18 “off” conditions; 10 dummy scans).

Quantification of fMRI Detection Power Using ROC Analysis

Given the fMRI stimulus paradigm, a *t*-test (27) was performed on the reconstructed SENSE fMR images to contrast the “on” and the “off” conditions. The detection powers of the regularized and unregularized SENSE reconstructions were computed using the ROC curves (28). For the experimental data, due to the lack of a “gold standard” for fMRI activation, we used the segmented EPI data with composition reconstruction to generate the relative gold standard of functional activation loci. The use of composition reconstruction for segmented EPI data ensured that the geometric distortion and susceptibility artifact were identical to the parallel MRI acquisition. All voxels with *t*-statistics above 4.0 ($P < 0.0001$) were considered to be the gold standard of functional activation. Note that once we decided the gold standard of functional activation, we did not change it during the ROC analysis. After we defined the gold standard of functional activation, we varied the threshold of *t*-statistics calculated from different

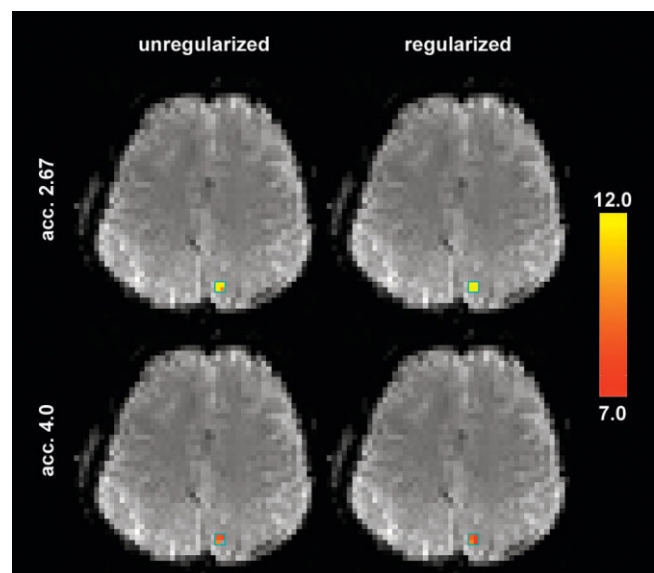


FIG. 3. The *t*-statistic maps from regularized and unregularized 2.67-fold/4.00-fold SENSE accelerations. The blue box indicates the location of the simulated fMRI BOLD contrast of 2%.

SENSE reconstructions to calculate TPR and FPR. Here the true-positive rate $TPR(\alpha)$ and false-positive rate $FPR(\alpha)$ of the detection thresholded at level α were calculated as

$$TPR(\alpha) = \frac{\text{size}(\text{area}(X_{SENSE} > \alpha) \cap \text{area}(X_{ref} > \alpha))}{\text{size}(\text{area}(X_{ref} > \alpha))}$$

$FPR(\alpha)$

$$= \frac{\text{size}(\text{area}(X_{SENSE} > \alpha) \cap (\text{area}(\text{brain}) - \text{area}(X_{ref} > \alpha)))}{\text{size}(\text{area}(\text{brain}) - \text{area}(X_{ref} > \alpha))}$$

[4]

where $\text{area}(X_{ref} > \alpha)$ indicates the t -statistic that is larger than α from the full-FOV reference fMRI time series, and $\text{area}(X_{SENSE} > \alpha)$ indicates the t -statistic that is larger than α from the SENSE fMRI reconstructions; $\text{area}(\text{brain})$ indicates the brain tissue in the image. \cap and $-$ denote the Boolean AND and NOT operators, respectively. The operator $\text{size}(\bullet)$ calculates the size of the area. ROC curves for both regularized and unregularized SENSE fMRI were calculated separately. The areas under each ROC curve were used to quantify the detection power. The false-positive rate was controlled below 10%. The area under the ROC curve was multiplied by 10.0 such that the maximum of the ROC area was 1.0. TPRs controlled at 1%, 5%, and 10% FPRs were also reported. EPI acquisitions with different EPI factors were calculated separately to generate ROC curves for different SENSE accelerations.

RESULTS

Simulations

Figure 3 shows the t -statistic maps of the simulation data (2% BOLD CNR) including both 2.67-fold and 4.00-fold SENSE accelerations with/without regularization. Both t -statistic maps were overlaid on the identical full-FOV reference EPI images. Note that with both acceleration rates, regularization improved the sensitivity of detection by achieving higher t -statistic values. At 2.67-fold acceleration with regularization, all four voxels of the implanted functional activation gave t -statistics above 12.0. With unregularized reconstructions, however, only three voxels had t -statistics above the value of 12.0. At 4.00-fold acceleration, the regularized SENSE reconstructions showed all four voxels with t -statistics above 7.0, while unregularized reconstructions had only three voxels exceeding the $t = 7.0$ threshold.

For more complete simulations, we varied the BOLD contrasts from 1%, 2%, 5%, to 10%. Figure 4a shows the averaged ROC analysis at different BOLD contrasts with a 4.00-fold SENSE acceleration, and 576 mm² simulated an active brain area (64 voxels). Note that higher BOLD contrasts yielded higher TPRs at 1%, 5%, and 10% controlled FPRs. At all BOLD contrasts, the regularized reconstructions had higher TPRs than unregularized reconstructions. At 10% BOLD contrast, the differences in TPRs were as large as 5% when FPRs were controlled below 10%. Figure 4b shows the simulation results with different sizes of simulated brain area with 5% BOLD contrast and 4.00-fold SENSE acceleration. Interestingly, the larger the simulated active brain area, the lower the TPR we calculated. This is

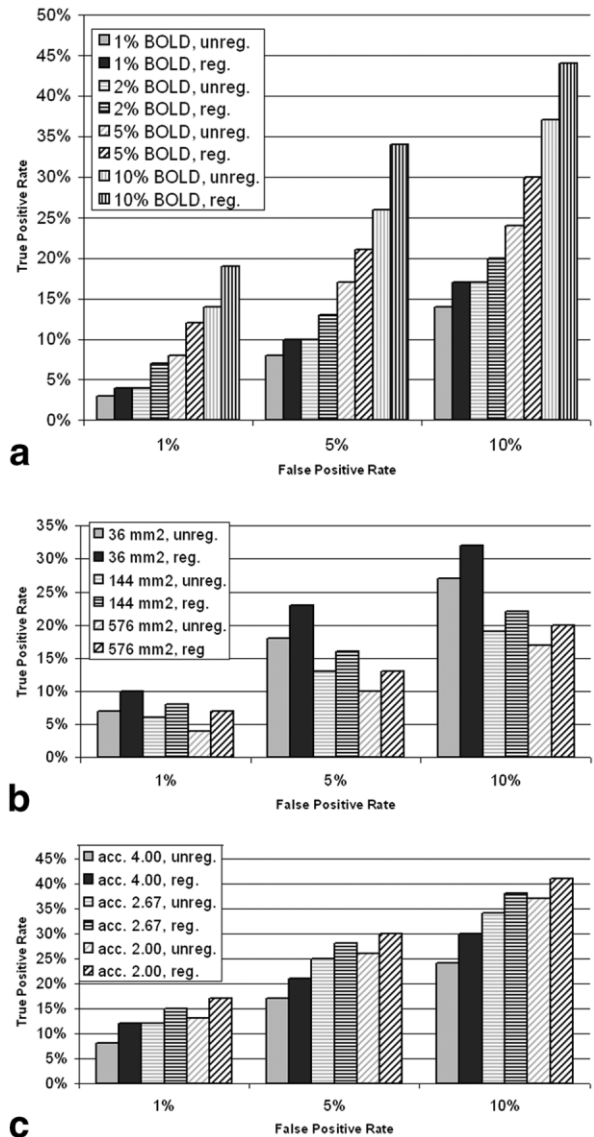


FIG. 4. **a:** ROC analysis for 1%, 2%, 5%, and 10% BOLD contrast in 4.00-fold SENSE acceleration and 576 mm² simulated active brain area. **b:** ROC analysis for 36 mm², 144 mm², and 576 mm² simulated active brain area with 4.00-fold SENSE acceleration and 5% BOLD contrast. **c:** ROC analysis for 2.00-, 2.67-, and 4.00-fold SENSE accelerations in 5% BOLD contrast and 576 mm² simulated active brain area.

because more specific and sensitive reconstructions are required to yield good TPRs in simulations with more simulated active brain voxels. Thus, when using the identical regularized and unregularized reconstructions, it is difficult to achieve simultaneous enhancement of specificity and sensitivity when more brain active voxels are simulated. Nevertheless, a comparison of the regularized and unregularized SENSE reconstructions indicated that regularization helped improve the detection power by providing higher TPRs at each controlled FPR. Lastly, Fig. 4c shows the ROC analysis results for different SENSE acceleration rates with a 5% BOLD contrast and a 576 mm² simulated active brain area (64 voxels). As expected, the higher SENSE acceleration

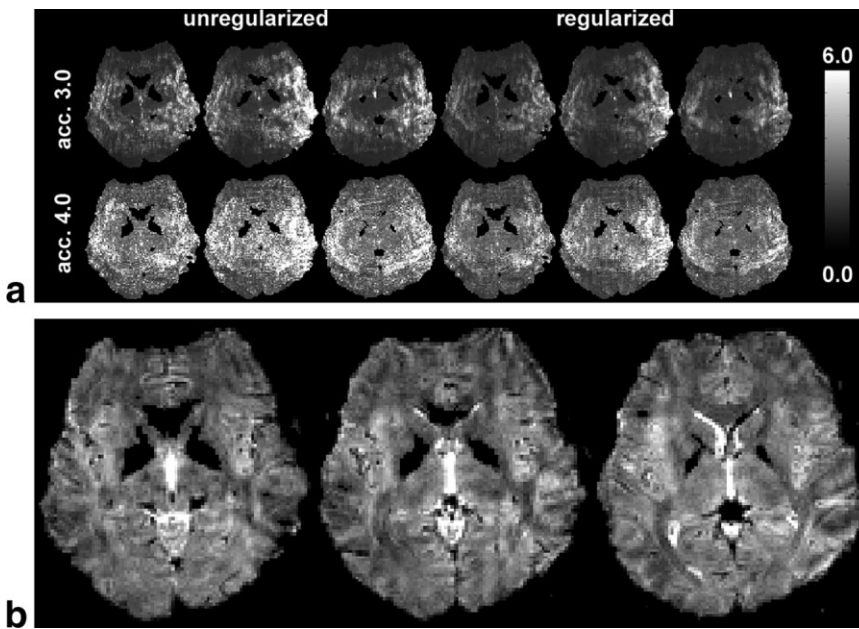


FIG. 5. **a:** g -Factor maps for 3.00- and 4.00-fold SENSE accelerations. An image mask covering the brain parenchyma was used to mask the g -factor maps to illustrate the spatial distribution of g -factors inside the brain. **b:** Reconstructed EPI SENSE images at 3.00-fold acceleration.

rate corresponded to a lower TPR at each FPR, potentially due to reduced data samples. A comparison of regularized and unregularized reconstructions showed that TPR was actually improved when regularization was employed. Regularization can improve TPR by 2–5%, depending on the SENSE acceleration rates and controlled FPRs.

3T Visual fMRI Experiment

For the 3T visual fMRI experiment, Fig. 5a shows the g -factor maps for 3.00-fold and 4.00-fold SENSE EPI. At 3.00-fold SENSE acceleration, without regularization, the averaged g -factor is 2.62 ± 1.47 (\pm SD). Regularization reduced the average g -factor to 2.21 ± 1.04 . In 4.00-fold acceleration, SENSE reconstructions without regularization gave the averaged g -factors of 3.67 ± 1.82 . Regularization reduced the averaged g -factor to 3.01 (SD = 1.26). Note that the g -factor maps are derived from the encoding matrix in the SENSE reconstruction. Using in vivo sensitivity, the coil maps in the encoding matrix are actually the full-FOV anatomical images. Thus it is possible that some residual ghosting artifacts in the anatomical image will affect the g -factor maps. However, g -factor maps contain more than just the coil sensitivity information. g -factor maps also include the spatial distribution of the condition-

ing of the encoding matrix, which is determined by the k -space trajectory in the accelerated scan and the physical locations of the array coils. Thus, we show EPI images in Fig. 5b to contrast the difference between g -factor maps and residual ghosting artifacts. A comparison of the g -factor maps and EPI images illustrates the difference between the two. Figure 6 shows the t -statistic maps of a 3T visual fMRI experiment using SENSE EPI with/without regularization at 3.00- and 4.00-fold accelerations. At 3.00-fold SENSE acceleration, regularized reconstructions yielded a larger functional activated area than the unregularized reconstructions around the occipital lobe (regularized: 2327 mm²; unregularized: 2139 mm²). Such an increase in sensitivity by regularization was also observed in the 4.00-fold SENSE acceleration (regularized: 896 mm²; unregularized: 735 mm²). Figure 7a shows the three aliased regions with 3.00-fold acceleration. One of the aliased regions is the visual cortex shown in Fig. 6. The corresponding time courses for all three aliased regions are depicted in Fig. 7b. Note that only activated visual cortex showed a time course that matched the stimulus paradigm. Two other aliased regions showed either low BOLD contrasts in all conditions or a time course that was mismatched to the stimulus paradigm. To illustrate both the

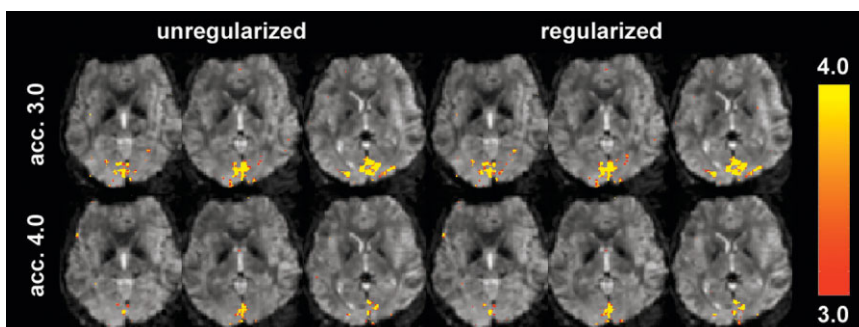
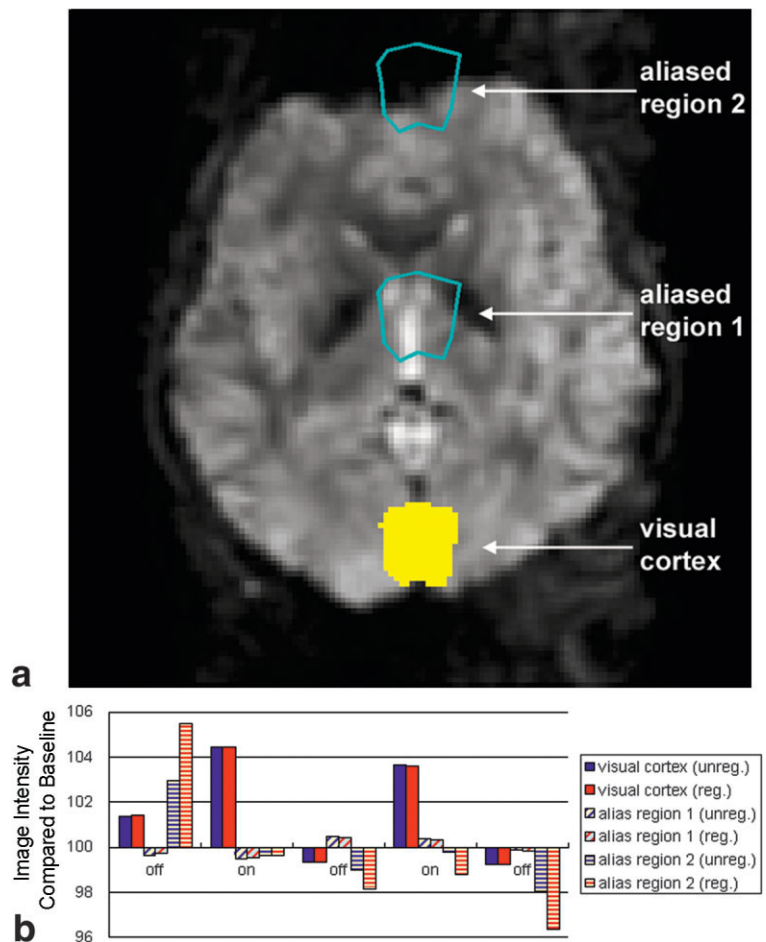


FIG. 6. The t -statistic maps of the visual fMRI experiment from a 3T scanner using an eight-channel head array, calculated with 3.00- or 4.00-fold SENSE acceleration.

FIG. 7. **a:** EPI image showing the three aliased regions with 3.00-fold acceleration. One of the aliased regions is the visual cortex. **b:** The time courses of the three regions. Note that only the visual cortex region time course corresponded well with the stimulus paradigm.



sensitivity and specificity of the SENSE reconstructions, Fig. 8 shows the ROC curves from t -statistic maps using 3.00- or 4.00-fold SENSE EPI acquisitions, including both regularized (solid lines) and unregularized (dashed lines) unfolding. We found that the detection power decreased when the SENSE acceleration increased from 3.00-fold to 4.00-fold. Using regularization to unfold the identical SENSE acceleration can improve the detection power in both 3.00- and 4.00-fold accelerations, as the ROC curves shift toward the upper-left corner. At FPR = 1%, regularization improved TPR by 6.7% and 28.2% for 3.00-fold and 4.00-fold accelerations, respectively. Regularization improved TPRs by 3.9% and 18.7% at FPR = 5% for 3.00- and 4.00-fold accelerations, respectively. Table 1 summarizes the ROC areas and TPRs at FPR = 1%, 5%, and 10%.

At 3.00-fold SENSE acceleration, the use of regularization can increase the ROC area maximally by 4.8% in SENSE unfolding. This implies that regularized SENSE reconstruction has a higher detection power than unregularized SENSE reconstructions. The same advantage of regularized SENSE reconstructions over unregularized ones was also observed in the 4.00-fold SENSE acquisitions. The use of regularization can increase the ROC area maximally by 16.4% in 4.00-fold acceleration.

1.5T Motor fMRI Experiment

For the 1.5T motor fMRI experiment, the t -statistic maps with full phase-encoding data and 2.00-fold SENSE acceleration are shown in Fig. 9. The contralateral motor cortex

Table 1

The Areas Under the ROC Curves and TPRs for the SENSE Reconstructions Using Traditional Algorithm (Unregularized) or Regularized Reconstructions in Visual fMRI Experiment at 3T with 3.0-fold or 4.0 Fold SENSE Acceleration*

SENSE acceleration	Reconstruction	TPR			ROC area
		FPR = 1%	FPR = 5%	FPR = 10%	
3.0	Unregularized	0.517	0.675	0.732	0.653
	Regularized	0.552	0.702	0.755	0.685
4.0	Unregularized	0.168	0.344	0.457	0.331
	Regularized	0.216	0.408	0.506	0.385

*The false positive rate of the ROC was controlled at 10%. The area was scaled by 10.0 such that the maximum of the area is 1.0.

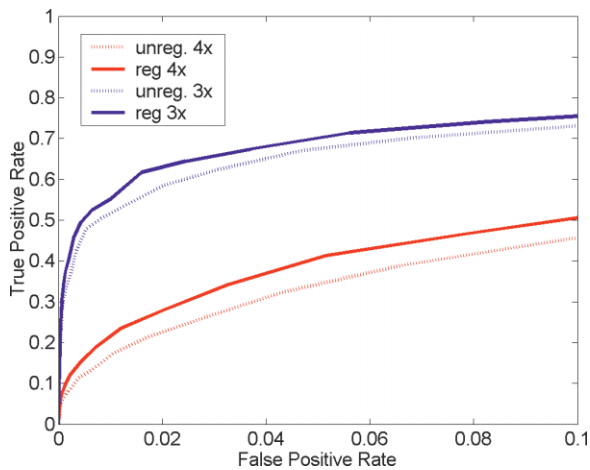


FIG. 8. The ROC curves for the 3.00- and 4.00-fold SENSE reconstructions using the traditional algorithm (unreg.) or regularized reconstruction (reg.) in a 3T visual fMRI experiment. The ROC curves were calculated based on the thresholded ($t = 4.0$) statistical values from composition reconstruction of the segmented EPI data with three and four EPI segments, respectively.

was found to be activated in both the full phase-encoding data and the 2.00-fold SENSE unfolding. Additional detected activation loci included the supplementary motor area and ipsilateral frontal cortex. Activation in these areas was consistently detected in both of the 2.00-fold SENSE reconstructions with/without regularization. Regularization increased the size of the active area in the t -statistic maps as compared to the unregularized SENSE reconstructions (regularized: 3751 mm²; unregularized: 3227 mm²). ROC curves for regularized and unregularized 2.00-fold SENSE accelerations are shown in Fig. 10. Using ROC analysis to quantify detection power, we found that regularization improved the TPR by 9.5% when FPR was controlled at 1% (unregularized TPR: 0.84, regularized TPR: 0.92). Regularization increased the area under the ROC curve 3.6% in 2.00-fold acceleration, compared to unregularized SENSE reconstructions. Table 2 summarizes the ROC areas from regularized and unregularized SENSE reconstructions in 2.00-fold acceleration.

DISCUSSION

A major finding of the current study is that regularization improves the CNR of an fMRI time series as the result of reduced contrast and a further reduced noise level. A concern with using prior information in dynamic imaging is that the replication of prior image features in time-series measurements may reduce the functional contrast. A reg-

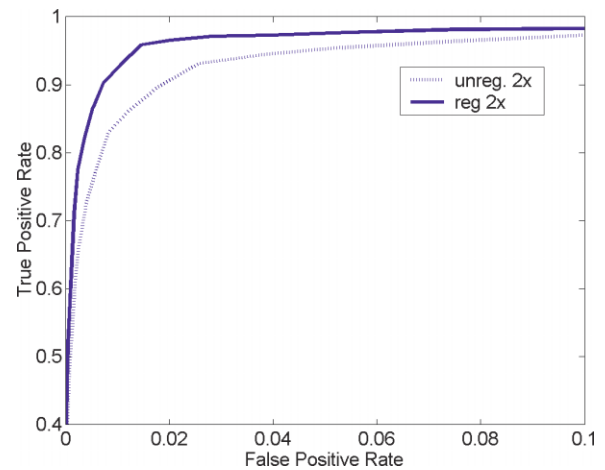


FIG. 10. The ROC curves for the 2.00-fold SENSE reconstructions using the traditional algorithm (unreg.) or regularized reconstruction (reg.) in a 1.5T motor fMRI experiment. The ROC curves were calculated based on the thresholded ($t = 4.0$) statistical values from composition reconstruction of two-segment segmented EPI.

ularized SENSE-EPI fMRI acquisition protocol was found to provide a robust CNR improvement in various scenarios, across field strengths (1.5T and 3T), across different coil array geometries (four- or eight-element circumferential head array), across different SENSE accelerations (from 2.00-fold to 4.00-fold accelerations), and across different functional modalities (visual and motor). From simulations and experimental data, we found that the functional CNR was actually improved by the regularized SENSE reconstruction compared to unregularized SENSE reconstructions. This suggests that the proposed regularization process suppresses the noise amplification in SENSE reconstruction to a greater extent than the possible functional contrast loss, by partially replicating prior image features. It was previously reported that SENSE acquisitions produced an SNR that was lower than full-FOV acquisitions but higher than theoretical predictions (14,16). This was partly explained by the influence of signal-dependent physiological noise (31,32). The improvement of the CNR reported in this work, however, was not related to physiological noise. This is because the SENSE reconstructions with/without regularization were calculated from identical segmented EPI data sets. Thus the improvement in CNR solely reflects the benefit of incorporating prior information in SENSE unfolding. In fact, the use of prior information can lead to a reduction of contrast between two functional states. However, the presented regularization technique further reduced the noise. Overall, the CNR was improved.

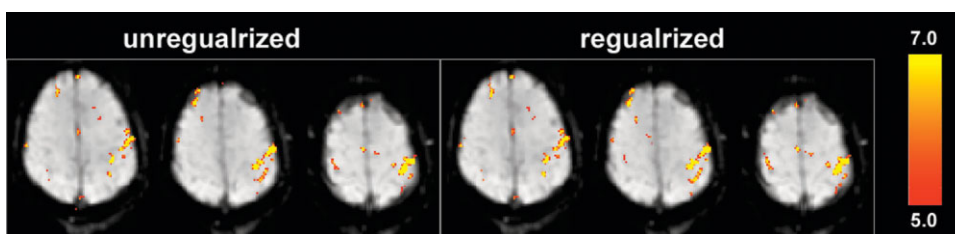


FIG. 9. The t -statistic maps of the motor fMRI experiment from a 1.5T scanner using a four-channel head array. The t -statistic maps were calculated from full phase-encoding data and 2.00-fold SENSE acceleration.

Table 2

The Areas Under the ROC Curves, and TPRs for the SENSE Reconstructions Using Traditional Algorithm (Unregularized) or Regularized Reconstructions in Motor fMRI Experiment at 1.5T with 2.0-fold SENSE Acceleration*

SENSE acceleration	Reconstruction	TPR			ROC area
		FPR = 1%	FPR = 5%	FPR = 10%	
2.0	Unregularized	0.844	0.952	0.973	0.934
	Regularized	0.925	0.976	0.983	0.968

*The false positive rate of the ROC was controlled at 10%. The area was scaled by 10.0 such that the maximum of the area is 1.0.

The major advantage of using parallel MRI (specifically SENSE MRI (10)) is that it can improve the spatiotemporal resolution of images (14,17). Additionally, it can reduce susceptibility artifacts and geometrical distortions due to the shortened readout window and increased phase-encoding bandwidth (15,16). Nevertheless, the price for these benefits is a reduced SNR and CNR in the functional images, as reported in previous visual (15,17) and motor (14–17) system studies. In this paper, we propose to mitigate the SNR and CNR loss in SENSE acquisitions by employing the information in full-FOV reference scans. In a previous study (20) we showed that the g -factors in a regularized SENSE reconstruction can be smaller than 1.0. This indicates that the regularized unfolding operation decreases the stochastic variability of the estimated spin density compared to the full-FOV reference scans. This noise reduction results from the prior knowledge used in the regularization process. Since prior information is employed in a regularized SENSE reconstruction, less variability of the estimated spin density from parallel acquisitions is expected. Thus, using regularization can partially compensate for the SNR loss due to the reduced samples in the accelerated acquisition.

The dependency of the static image in the regularized SENSE reconstruction on the dynamic time series, such as fMRI data, is similar to that in the keyhole imaging technique (29,30), which replicates the center part of the k -space in the dynamic scan in order to enhance the temporal resolution of data acquisition. In contrast to keyhole imaging, regularized SENSE reconstruction focuses on the stabilization of the matrix inversion during restoration of the full-FOV unaliased image. Keyhole imaging cannot be applied directly to reduce the noise amplification, as in regularized SENSE reconstruction, because the keyhole technique applies the static lower-resolution image to the full-FOV unaliased image, which is not available until the necessary image unfolding process is completed. We would also like to clarify that the inclusion of prior information in SENSE reconstruction does not represent a mere DC shift in all time series images. The matrix solution of the prior-informed regularized reconstruction (20) indicates that the prior information is not superimposed on the time series directly. Actually, the prior is used as a combination of the DC shift (from the prior information) and matrix conditioning (on the inversion of encoding matrix).

Previous studies applied parallel MRI acquisition protocols to fMRI experiments using the PRESTO (17) and gradient-echo EPI (14–16) sequences. The purpose of using SENSE MRI as the fMRI data acquisition protocol is to enhance spatiotemporal resolution by reducing the time required to traverse k -space. Thus, single-shot EPI or re-

duced phase-encoding PRESTO have become feasible on high-field ($\geq 3T$) scanners, where the T_2^* relaxation time of human gray matter may be shorter than 30 ms in areas with pronounced field inhomogeneities (33,34). Traditionally, such a short T_2^* made single-shot EPI unsuitable for sufficient spatiotemporal resolution because of the insufficient acquisition time to completely traverse k -space. With parallel imaging, the time required to traverse k -space is reduced by “unfolding” the aliased images from individual receivers in the array. The reduced k -space traversing time also helps reduce susceptibility artifacts and geometric distortions originating from the local magnetic field inhomogeneity. This is due to the shortened readout time of the data acquisition, which contributes less to local spin dephasing within individual voxels. Geometric distortion is also improved by a higher bandwidth in the phase-encoding direction. Another significant benefit of SENSE is that the SENSE EPI may reduce the acoustic noise by reduced switching of the gradients to complete k -space trajectory traversing (13).

In this study we utilized the “in vivo sensitivity” reconstruction approach described by Sodickson (23). This method substitutes full-FOV array element images from the reference scan in place of the estimated coil profile used by SENSE (10). Thus a misestimation of the coil sensitivity profile is avoided. One major disadvantage of the in vivo sensitivity reconstruction approach is that it cannot reconstruct the image features that are not present in the full-FOV reference scans. This situation occurs when the reference scan and the SENSE-accelerated scans involve time-varying anatomical features, such as cardiac imaging at different phases. However, this issue is less critical in brain imaging, since it has been reported that the cerebral cortex stays relatively stationary even in the presence of cardiac pulsation (35). Thus, the in vivo sensitivity reconstruction approach is capable of revealing most of the anatomical and functional features in each time point of the dynamic scan of the brain.

One advantage of using in vivo sensitivity is the simplicity of prior image specifications. The difference in the prior image for regularized SENSE reconstructions using either in vivo sensitivity or conventional coil sensitivity map estimates (e.g., the ratio between array coil images and body coil images) is that by using the in vivo sensitivity, all pixels in the prior image have values of 1.0. With conventional coil sensitivity map estimates, the prior image is a full-FOV image with anatomical features. In the conventional coil sensitivity approach, such a prior image should contain only anatomical features, *without* spatial modulation from the coil sensitivity profile. Even though we can use the traditional sum-of-squares to combine all

channels of the array coils to yield a full-FOV prior image, such a combined image will still contain residual spatial modulation of the coil sensitivity maps, and thus it cannot serve as a good prior image. However, with the *in vivo* sensitivity approach, we do not require such a full-FOV image with anatomical features and without spatial modulation of the coil sensitivity maps. In *in vivo* sensitivity method, the use of a constant prior image with a pixel value equal to 1.0 can avoid potential errors and bias from the specification of prior information in the SENSE reconstruction.

Using regularization in SENSE reconstructions, we require aliased accelerated image, prior full-FOV image, and coil sensitivity maps to compute the regularization parameters. Investigators traditionally have used a full-FOV reference image to estimate the coil sensitivity maps. However, in our approach we do not estimate the coil sensitivity profile because, as indicated in Eq. [2], fMRI experiments mostly focus on the dynamic BOLD contrast *within* an image voxel to differentiate between active and baseline brain states. The *in vivo* sensitivity method serves this purpose. In fact, this is another advantage of using *in vivo* sensitivity in fMRI experiments, in addition to the advantages of using prior image specification and avoiding coil map estimation errors, as described above. Note that when we use *in vivo* sensitivity, the coil sensitivity maps are identical to the full-FOV reference image. However, if investigators use the conventional coil sensitivity estimated from the ratio between the body- and array-coil full-FOV reference images, the regularization parameters will differ from those of the *in vivo* sensitivity method.

The acquisition protocol presented in this paper is based on the segmented EPI sequence, similarly to the temporal SENSE (TSENSE) (16,25) and unaliasing by Fourier-encoding the overlaps using the temporal dimension (UNFOLD) (36,37) techniques. We demonstrated with simulations and experimental data that each interleaved segment of EPI can be unfolded into a full-FOV image with spatial resolution that is identical to an image reconstructed by combining all segments. Using parallel imaging reconstruction, we can increase the temporal resolution when the individual EPI segment is reconstructed into a full-FOV image. The increment in the number of observations can improve the detection power. It should be noted that the proposed regularization procedure can also be incorporated using a number of variations in the segmented EPI sequences, including variable density sampling (25,38,39), to improve the SNR and CNR in fMRI studies.

One practical concern with applying the regularized SENSE reconstruction is the computational load. Currently, the bottleneck in the computational performance of SENSE fMRI is caused by the unfolding of the SENSE accelerated scans, not the time required to estimate the regularization parameters. We noticed that once the regularization parameters were determined, the computational reconstruction time was identical to that of reconstruction without regularization. Thus the additional computational time required for the proposed technique is not excessive. In dynamic imaging, the impact on the increased image reconstruction time due to regularization estimation can be minimized by estimating regularizations only once and

then applying identical regularization parameters to multiple measurements. The computational performance can be further improved with the use of 1) compiled language for the code, 2) the direct regularization approach to estimate the time required to estimate the regularization parameters, and 3) the complex conjugated approach for SENSE unfolding. In addition to the L-curve technique used in this study, other automatic regularization estimation methods, such as generalized cross validation (GCV) (40,41), potentially can be used to estimate appropriate regularization parameters.

CONCLUSIONS

In comparison with conventional EPI scans, parallel imaging techniques can reduce susceptibility artifacts and image geometric distortions, and improve the spatiotemporal resolution in fMRI studies. In this paper we have presented a regularized SENSE fMRI method based on Tikhonov regularization to mitigate the SNR and CNR loss due to geometric correlation in the spatial information from the array coil elements. With the use of an eight-channel head array, parametric simulations with different BOLD contrasts (1–10%), SENSE acceleration rates (2.00- to 4.00-fold), and sizes of the active brain area (36–576 mm²) showed that the detection power was improved when regularization was employed in SENSE fMRI acquisitions. Additional experimental data at 1.5T and 3T with four- and eight-channel arrays for motor and visual fMRI experiments validate that the proposed regularization procedure can improve the sensitivity and specificity of SENSE fMRI to detect brain activation.

ACKNOWLEDGMENT

We thank Dr. Walid Kyriakos for providing the RF array coil at Brigham and Women's Hospital.

REFERENCES

- Belliveau JW. Functional NMR imaging of the brain. Ph.D. dissertation, Harvard University, Cambridge, MA, 1990.
- Belliveau JW, Kennedy DN, McKinstry RC, Buchbinder BR, Weisskoff RM, Cohen MS, Vevea JM, Brady TJ, Rosen BR. Functional mapping of the human visual cortex by magnetic resonance imaging. *Science* 1991; 254:716–719.
- Belliveau JW, Kennedy DN, McKinstry RC, Buchbinder BR, Weisskoff RM, Vevea JM, Nadeau K, Cohen MS, Brady TJ, Rosen BR. Functional mapping of the human visual cortex with susceptibility-contrast MR imaging. *J Magn Reson Imaging* 1991;1:202.
- Ogawa S, Lee TM, Kay AR, Tank DW. Brain magnetic resonance imaging with contrast dependent on blood oxygenation. *Proc Natl Acad Sci USA* 1990;87:9868–9872.
- Kwong KK, Belliveau JW, Chesler DA, Goldberg IE, Weisskoff RM, Poncelet BP, Kennedy DN, Hoppel BE, Cohen MS, Turner R, Cheng HM, Brady TJ, Rosen BR. Dynamic magnetic resonance imaging of human brain activity during primary sensory stimulation. *Proc Natl Acad Sci USA* 1992;89:5675–5679.
- Mansfield P. Multi-planar image formation using NMR spin echos. *J Physics* 1977;C10:L55–L58.
- Schmitt F, Stehling MK, Turner R, Bandettini PA. Echo-planar imaging: theory, technique, and application. Berlin/New York: Springer; 1998. xiv, 662 p.
- Roemer PB, Edelstein WA, Hayes CE, Souza SP, Mueller OM. The NMR phased array. *Magn Reson Med* 1990;16:192–225.

9. Sodickson DK, Manning WJ. Simultaneous acquisition of spatial harmonics (SMASH): fast imaging with radiofrequency coil arrays. *Magn Reson Med* 1997;38:591–603.
10. Pruessmann KP, Weiger M, Scheidegger MB, Boesiger P. SENSE: sensitivity encoding for fast MRI. *Magn Reson Med* 1999;42:952–962.
11. Bammer R, Keeling SL, Augustin M, Pruessmann KP, Wolf R, Stollberger R, Hartung HP, Fazekas F. Improved diffusion-weighted single-shot echo-planar imaging (EPI) in stroke using sensitivity encoding (SENSE). *Magn Reson Med* 2001;46:548–554.
12. Weiger M, Pruessmann KP, Boesiger P. 2D SENSE for faster 3D MRI. *MAGMA* 2002;14:10–19.
13. de Zwart JA, van Gelderen P, Kellman P, Duyn JH. Reduction of gradient acoustic noise in MRI using SENSE-EPI. *Neuroimage* 2002;16:1151–1155.
14. Preibisch C, Pilatus U, Bunke J, Hoogenraad F, Zanella F, Lanfermann H. Functional MRI using sensitivity-encoded echo planar imaging (SENSE-EPI). *Neuroimage* 2003;19(2 Pt 1):412–421.
15. Weiger M, Pruessmann KP, Osterbauer R, Bornert P, Boesiger P, Jezzard P. Sensitivity-encoded single-shot spiral imaging for reduced susceptibility artifacts in BOLD fMRI. *Magn Reson Med* 2002;48:860–866.
16. de Zwart JA, van Gelderen P, Kellman P, Duyn JH. Application of sensitivity-encoded echo-planar imaging for blood oxygen level-dependent functional brain imaging. *Magn Reson Med* 2002;48:1011–1020.
17. Golay X, Pruessmann KP, Weiger M, Crelier GR, Folkers PJ, Kollias SS, Boesiger P. PRESTO-SENSE: an ultrafast whole-brain fMRI technique. *Magn Reson Med* 2000;43:779–786.
18. Sodickson DK, McKenzie CA. A generalized approach to parallel magnetic resonance imaging. *Med Phys* 2001;28:1629–1643.
19. Tikhonov AN, Arsenin VI. Solutions of ill-posed problems. Washington/New York: Winston/Halsted Press; 1977. xiii, 258 p.
20. Lin FH, Kwong KK, Belliveau JW, Wald LL. Parallel imaging reconstruction using automatic regularization. *Magn Reson Med* 2004;51:559–567.
21. Hansen PC. Rank-deficient and discrete ill-posed problems: numerical aspects of linear inversion. Philadelphia: SIAM; 1998. xvi, 247 p.
22. Yacoub E, Shmuel A, Pfeuffer J, Van De Moortele PF, Adriany G, Andersen P, Vaughan JT, Merkle H, Ugurbil K, Hu X. Imaging brain function in humans at 7 Tesla. *Magn Reson Med* 2001;45:588–594.
23. Sodickson DK. Tailored SMASH image reconstructions for robust in vivo parallel MR imaging. *Magn Reson Med* 2000;44:243–251.
24. McKinnon GC. Ultrafast interleaved gradient-echo-planar imaging on a standard scanner. *Magn Reson Med* 1993;30:609–616.
25. Kellman P, Epstein FH, McVeigh ER. Adaptive sensitivity encoding incorporating temporal filtering (TSENSE). *Magn Reson Med* 2001;45:846–852.
26. Madore B. UNFOLD-SENSE: a parallel MRI method with self-calibration and artifact suppression. *Magn Reson Med* 2004;52:310–320.
27. Friston KJ, Holmes AP, Poline JB, Grasby PJ, Williams SC, Frackowiak RS, Turner R. Analysis of fMRI time-series revisited. *Neuroimage* 1995;2:45–53.
28. Chow S-C, Shao J. Statistics in drug research: methodologies and recent developments. New York: M. Dekker; 2002. xiv, 367 p.
29. van Vaals JJ, Brummer ME, Dixon WT, Tuithof HH, Engels H, Nelson RC, Gerety BM, Chezmar JL, den Boer JA. “Keyhole” method for accelerating imaging of contrast agent uptake. *J Magn Reson Imaging* 1993;3:671–675.
30. Hu X. On the “keyhole” technique. *J Magn Reson Imaging* 1994;4:231.
31. Kruger G, Kastrup A, Glover GH. Neuroimaging at 1.5 T and 3.0 T: comparison of oxygenation-sensitive magnetic resonance imaging. *Magn Reson Med* 2001;45:595–604.
32. Kruger G, Glover GH. Physiological noise in oxygenation-sensitive magnetic resonance imaging. *Magn Reson Med* 2001;46:631–637.
33. Chen NK, Egorova S, Guttman CR, Panych LP. Functional MRI with variable echo time acquisition. *Neuroimage* 2003;20:2062–2070.
34. Barth M, Metzler A, Klarhofer M, Roll S, Moser E, Leibfritz D. Functional MRI of the human motor cortex using single-shot, multiple gradient-echo spiral imaging. *Magn Reson Imaging* 1999;17:1239–1243.
35. Poncelet BP, Wedeen VJ, Weisskoff RM, Cohen MS. Brain parenchyma motion: measurement with cine echo-planar MR imaging. *Radiology* 1992;185:645–651.
36. Madore B, Glover GH, Pelc NJ. Unaliasing by Fourier-encoding the overlaps using the temporal dimension (UNFOLD), applied to cardiac imaging and fMRI. *Magn Reson Med* 1999;42:813–828.
37. Madore B. Using UNFOLD to remove artifacts in parallel imaging and in partial-Fourier imaging. *Magn Reson Med* 2002;48:493–501.
38. Jakob PM, Griswold MA, Edelman RR, Sodickson DK. AUTO-SMASH: a self-calibrating technique for SMASH imaging. Simultaneous acquisition of spatial harmonics. *MAGMA* 1998;7:42–54.
39. Heidemann RM, Griswold MA, Haase A, Jakob PM. VD-AUTO-SMASH imaging. *Magn Reson Med* 2001;45:1066–1074.
40. Golub GH, Heath MT, Wahba G. Generalized cross-validation as a method for choosing a good ridge parameter. *Technometrics* 1979;21:215–223.
41. Wahba G. Practical approximate solutions to linear operator equations when the data are noisy. *SIAM J Numer Anal* 1977;14:651–667.